Hybrid-Channel Estimation in Extra-Large MIMO Systems via Regularized Sparse Bayesian Learning

Hamza Djelouat, and Markku Juntti
Centre for Wireless Communications
University of Oulu
Oulu, Finland

Mikko J. Sillanpää
Research Unit of Mathematical Sciences
University of Oulu
Oulu, Finland

Bhaskar D. Rao
ECE Department
University of California San Diego
California, USA

***Abstract*—This paper investigates channel estimation for extra-large multi-input multi-output (XL-MIMO) systems, where the large antenna array aperture extends the near-field propagation region, thus leading to a hybrid channel propagation model that accounts for both far-field and near-field components. The latter will exhibit a sparse channel representation with a hybrid sparsity structure, which renders channel estimation extremely challenging. To this end, the paper proposes a novel approach that exploits both sparse Bayesian learning (SBL) and the total variation (TV) penalty with an adaptive weight to incorporate the hybrid-sparse structure. The proposed tune-free iterative algorithm dynamically adjusts the regularization weight, effectively distinguishing between block-sparse and individual sparse components in the hybrid channel representation. Extensive numerical simulations validate the performance and robustness of the proposed approach, demonstrating significant improvements in channel estimation under near-field propagation conditions.**

I. Introduction

Extremely large-scale multiple-input multiple-output (XL-MIMO) technology has emerged as a fundamental enabler for next-generation wireless communications [1]. These systems promise remarkable enhancements in spectral and energy efficiency, dramatically increased data rates, and highly reliable massive access capabilities [2], [3]. While XL-MIMO communications offer huge benefits, they introduce challenges from distinctive electromagnetic propagation characteristics. Importantly, the near-field region can extend hundreds of meters. This means scatterers and UEs frequently reside within the BS's near-field—at distances below the Rayleigh boundary between near and far-field regions. Under these conditions, EM wave propagation requires spherical wave models rather than conventional plane wave approximations.

In realistic XL-MIMO communications environments, channels typically exhibit hybrid-field characteristics: certain scatterers are positioned in the far-field of the BS, while others are located in the near-field. Consequently, depending on the spatial distribution of the BS, scatterers, and UEs, both far-field and near-field propagation paths coexist, collectively constituting a hybrid-field channel. This distinctive feature necessitates that channel estimation algorithms for XL-MIMO systems accommodate both propagation regimes while maintaining robustness against variable channel conditions.

To fully leverage XL-MIMO systems, accurate CSI estimation with minimal signaling overhead is essential. The channel sparsity can be exploited to simplify the channel estimation. For far-field channels, angular domain sparsity has been widely exploited to develop efficient estimators, including non-uniform burst sparse Bayesian learning (SBL) [4], message passing algorithms [5], and simultaneous orthogonal matching pursuit (SOMP) [3]. However, near-field propagation presents unique challenges, as an angular domain transformation fails to provide highly sparse channel representations, instead yielding block-sparse representations [3]. To address this limitation, Cui *et al.* [3] introduced the polar domain representation, capturing both distance and angular information, resulting in significantly improved sparsity. This has led to numerous solutions from both CS theory [6], [3] and deep learning approaches [7], [8].

Recent research efforts have increasingly focused on addressing the hybrid-channel model [9], [10], [11], [12], [13], [14]. Wei *et al.* proposed a two-stage OMP algorithm that sequentially estimates far-field and near-field components, assuming prior knowledge of the numbers of their respective path components. To eliminate the necessity for prior knowledge about the proportion of near-field and far-field path components, Yang *et al.* used the norm of residual vector as a criterion to identify the nature of the propagation path [12]. On the other hand, Yan *et al.* developed a path classification algorithm based on the angular beam-width of the channel to distinguish between far-field and near-field components. Once the path type has been detected, both approaches apply an OMP-based method to estimate the channel. While the explicit knowledge of the channel composition is not required, the channel estimation quality is limited by the typically inferior performance of the OMP-based algorithms compared to the Bayesian-based solutions [15].

This paper addresses the channel estimation problem in XL-MIMO systems from a Bayesian perspective. Specifically, we adopt the angular domain transformation of the channel, leveraging its hybrid sparsity structure, namely block sparsity, representing the near-field components and individual spikes corresponding to the far-field components. To handle this hybrid sparsity structure, we formulate the problem as an SBL-based optimization problem augmented with a prior function that captures the essence of the hybrid-sparsity model. The proposed formulation combines two regularization terms: i) total variation (TV) to promote block sparsity and ii) log-determinant (log-det) regularizer to encourage individual spar-

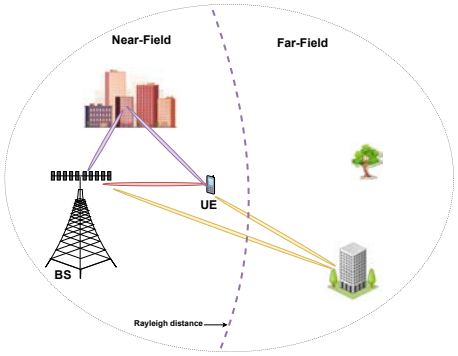

Fig. 1: The hybrid-field communication system for XL-MIMO.

sity. Additionally, an adaptive regularization mechanism is introduced to distinguish between different sparsity profiles. Simulation results demonstrate that the proposed channel estimation quality across various scenarios compared to the state-of-the-art benchmarks.

II. System Model

This paper considers a single-cell network comprising a multi-antenna base station (BS) equipped with an extremely large-scale uniform linear array (ULA) equipped with N antennas serving K single antenna UEs.

A. Channel Model

The Rayleigh distance, which defines the boundary between far-field and near-field regions, is given by $D_{\text{Rayleigh}} = \frac{2D^2}{\lambda_{\text{c}}}$, where D is the array aperture and λ_{c} denotes the carrier wavelength. Due to the large aperture of the XL-ULA, the Rayleigh distance can extend to hundreds of meters. This distinctive characteristic means that both scatterers and connected UEs can be located in either the near-field region or the far-field region, leading to different signal propagation characteristics. Subsequently, the *hybrid channel* model can be given as

$$\mathbf{h} \quad = \mathbf{h}_{\text{f}} + \mathbf{h}_{\text{n}}. \tag{1}$$

The hybrid channel model (1) comprises both far-field and near-field components, each with dynamically varying parameters, making the channel conditions highly variable. Indeed, since the wavefront characteristics differ significantly between the two regions—approximately planar in the far-field and spherical in the near-field—the array responses for each region must be modeled separately.

1) Far-Field Channel Model: Assuming that the UE and the scatterers are static and located in the far-field region of the BS, the multi-path far-field channel response is modeled based on the planar wavefront assumption as

$$\mathbf{h}_{\text{f}} = \sqrt{\frac{1}{P_{\text{f}}}} \sum_{p=1}^{P_{\text{f}}} g_p \mathbf{a}_{\text{f}}\big(\phi_p\big). \tag{2}$$

where P_{f} denotes the the number of far-field paths, while g_p, and ϕ_p represent the complex path gain, and the angle associated with the pth path, respectively. The steering vector $\mathbf{a}_{\text{f}}(\cdot)$ is given as [16]

$$\mathbf{a}_{\text{f}}\big(\phi_{\mathbf{p}}\big) = \frac{1}{\sqrt{N}}\big[1, e^{-2j\pi \sin(\phi_p)}, \ldots, e^{-2j(N-1)\sin(\phi_p)}\big]^{\text{T}},$$

where d represents the normalized spacing between the adjacent antenna elements at the BS.

2) Near-Field Channel Model: When the UE is located in the near-field region of the BS, the channel response is usually assumed to follow the spherical wavefront assumption [3] as

$$\mathbf{h}_{\text{n}} = \sqrt{\frac{1}{P_{\text{n}}}} \sum_{p=1}^{P_{\text{n}}} g_p \mathbf{a}_{\text{n}}\big(\phi_l, r_p\big), \tag{3}$$

where P_{n} denotes the the number of near-field paths, and r_p denotes the distance associated with the pth path to the reference antenna at the BS, respectively. The steering vector $\mathbf{a}_{\text{n}}\big(\boldsymbol{\phi}_p, r_p\big)$ is given as

$$\mathbf{a}_{\text{n}}\big(\boldsymbol{\phi}_p, r_p\big) = \big[1, e^{-jk_{\text{c}}(r_p^{(1)} - r_p)}, \ldots, e^{-jk_{\text{c}}(r_p^{(N-1)} - r_p)}\big]^{\mathsf{T}},$$

where $k_{\text{c}} = \frac{2\pi f_{\text{c}}}{c}$, where f_{c} denotes the carrier central frequency and $r_{\text{l}}^{(n)} = \sqrt{r^2 + \sigma_{\text{n}}^2 d^2 - 2r_{\text{l}}\sigma_{\text{n}} d\theta_{\text{l}}}$ denotes the distance from the nth scatterer to the nth BS antenna, and $\sigma_{\text{n}} = \frac{2n-N-1}{2}$ with $n = 1, \ldots, N$ [3].

B. Problem Formulation

In the down-link channel estimation, the BS transmits known pilot signals to the UEs for T time slots. We assume that orthogonal pilots are adopted and consider an arbitrary UE without loss of generality. The BS transmits a pilot signal $\mathbf{w}_t$ at time instance t to the UE, subsequently, the pilot signal is given as

$$y_t = \mathbf{h}_t^{\text{H}} \mathbf{w}_t + n_t, \quad t = 1, \cdots, T. \tag{4}$$

Let us denote the received signal over T symbols as $\mathbf{y} = [y_1, \ldots, y_{\text{T}}]^{\text{T}}$, and define the pilot matrix $\mathbf{W} = [\mathbf{w}_1, \ldots, \mathbf{w}_{\text{T}}]^{\text{T}} \in \mathbb{C}^{T \times N}$, and the noise vector $\mathbf{n} = [n_1, \ldots, n_{\text{T}}]^{\text{T}} \in \mathbb{C}^T \sim \mathcal{CN}(0, \sigma^2 I_{\text{T}})$. Subsequently, we can write the received signal as

$$\mathbf{y} = \mathbf{W}\mathbf{h} + \mathbf{n}, \tag{5}$$

Based on (5), the channel estimation problem is conventionally formulated as an inverse problem to recover $\mathbf{h}$ from the received pilot signal $\mathbf{y}$. To minimize the signaling overhead, the pilot length is deliberately chosen to be significantly smaller than the number of the BS antennas, i.e., $T \ll N$. This constraint transforms the channel estimation in (5) into an ill-posed problem. However, owing to the channel sparsity under appropriate transforms [4], [9], channel estimation has been effectively formulated as a sparse recovery problem. The existing works rely heavily on the channel sparsity to design compressed sensing algorithms for channel estimation. However, the existing solution applies sparsifying transformations to far- and near-field paths independently, resulting in an incompatible hybrid sparsity pattern. To address this, we propose a unified representation that enables an efficient solution for hybrid channel estimation in XL-MIMO.

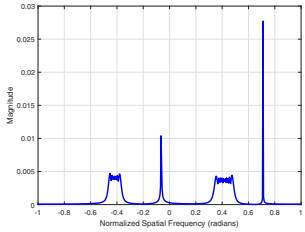

Fig. 2: Angular Domain Representation for a channel with $P_{\mathrm{f}} = 2$ and $P_{\mathrm{n}} = 2$.

III. Proposed Bayesian Solution

Aiming at a solution under the CS framework, we adopt the angular domain representation of the channel and rewrite the received signal as

$$\mathbf{y} = \mathbf{W}\mathbf{F}\mathbf{z} + \mathbf{n} = \mathbf{\Psi}\mathbf{z} + \mathbf{n}. \tag{6}$$

where $\mathbf{h} = \mathbf{F}\mathbf{z}$ such that $\mathbf{F} \in \mathbb{C}^{N\times N}$ denotes the unitary Fourier transform matrix and $\mathbf{z} \in \mathbb{C}^N$ is the *sparse* angular representation vector of the channel $\mathbf{h}$ in the angular domain. Therefore, based on (6), the hybrid near/far-filed channel estimation problem can be converted into a sparse signal recovery problem whose objective is to recover the sparse vector $\mathbf{z}$ from the noisy measurement $\mathbf{y}$.

To solve the above problem within a Bayesian framework, we construct a probabilistic model of the inference problem by treating the *unknown* vector $\mathbf{z}$ as a random variable with an associated probability density function (PDF). For analytical tractability, we model $\mathbf{z}$ as a zero-mean multivariate complex Gaussian distribution:

$$\mathbf{z} \sim \mathcal{CN}(\mathbf{0}, \mathrm{diag}(\boldsymbol{\alpha})), \tag{7}$$

where $\boldsymbol{\alpha} = [\alpha_1, \ldots, \alpha_N]^{\mathrm{T}} \in \mathbb{R}_+^N$ represents the *hyper-parameter vector* controlling the variance of each element in $\mathbf{z}$. Due to the additive Gaussian nature of the noise, the posterior density $p(\mathbf{z}|\mathbf{y};\boldsymbol{\alpha})$ is also Gaussian, given by:

$$p(\mathbf{z}|\mathbf{y};\boldsymbol{\alpha}) \sim \mathcal{CN}(\boldsymbol{\mu}, \boldsymbol{\Sigma}), \tag{8}$$

where

$$\boldsymbol{\mu} = \frac{1}{\sigma^2}\boldsymbol{\Sigma}\mathbf{\Psi}^{\mathrm{H}}\mathbf{y}, \quad \boldsymbol{\Sigma} = \left(\frac{1}{\sigma^2}\mathbf{\Psi}^{\mathrm{H}}\mathbf{\Psi} + \mathrm{diag}(\boldsymbol{\alpha})^{-1}\right)^{-1}. \tag{9}$$

It is evident from (9) that for known values of $\boldsymbol{\alpha}$ and $\mathbf{\Psi}$, the maximum a posteriori estimate of $\mathbf{z}$ is $\boldsymbol{\mu}$. Therefore, the aim of the proposed solution is to estimate the hyperparameter vector $\boldsymbol{\alpha}$. Inspired by the SBL approach, we obtain the MAP estimate $\hat{\boldsymbol{\alpha}}$ by maximizing the posterior density function $p(\boldsymbol{\alpha}|\mathbf{y})$ with respect to $\boldsymbol{\alpha}$, resulting in the non-convex problem:

$$\begin{aligned}\hat{\boldsymbol{\alpha}} &= \underset{\boldsymbol{\alpha}\succeq 0}{\mathrm{argmax}} \log p(\boldsymbol{\alpha}|\mathbf{y}) \\ &= \underset{\boldsymbol{\alpha}\succeq 0}{\mathrm{argmin}} \log\det\left(\boldsymbol{\Sigma}_{\mathrm{y}}\right) + \mathbf{y}^{\mathrm{H}}\boldsymbol{\Sigma}_{\mathbf{y}}^{-1}\mathbf{y} - \log p(\boldsymbol{\alpha}),\end{aligned} \tag{10}$$

where $\boldsymbol{\Sigma}_{\mathrm{y}} = \sigma^2\mathbf{I} + \mathbf{\Psi}\mathrm{diag}(\boldsymbol{\alpha})\mathbf{\Psi}^{\mathrm{H}}$ and $\log p(\boldsymbol{\alpha})$ is a prior function that should be ideally designed to express the prior belief on the structure of the hyper-parameter vector $\boldsymbol{\alpha}$.

This paper builds upon the approach used in our preliminary work [17] to tackle the channel estimation problem in hybrid-channel XL-MIMO systems. For completeness, we provide a comprehensive explanation of the proposed solution. First, we discuss the design of the prior function $p(\boldsymbol{\alpha})$, followed by a detailed derivation of the hyperparameter vector $\boldsymbol{\alpha}$ estimation using the SBL framework and the Alternating Direction Method of Multipliers (ADMM) algorithm.

A. Design of $p(\boldsymbol{\alpha})$

Since both near-field and far-field components are present in the signal, $\mathbf{z}$ exhibits a hybrid sparsity pattern. Specifically, $\mathbf{z}$ consists of isolated spikes corresponding to far-field components and a non-uniform block of nonzero elements associated with near-field components, as shown in Fig. 2.

To capture the hybrid structures effectively, the prior function $p(\boldsymbol{\alpha})$ needs to be designed to enforce an estimate consisting of both isolated spikes and nonzero element blocks. The current Bayesian approaches include hard coupling of hyperparameters [18] and TV penalties [19]. While effective for block sparse recovery with unknown block partition, it struggles with hybrid sparse patterns as it penalizes the transition between every pair equally. To this end, we utilize the following hyper-prior function:

$$-\log p(\boldsymbol{\alpha}) = \sum_{i=2}^{N}\sum_{j\in\Omega_i} \beta_{i,j}|\log(\alpha_i) - \log(\alpha_j)|, \tag{11}$$

where Ω_i is the set of neighboring elements of the z_i, and $\beta_{i,j} \in [0,1]$ represents an adaptive regularization weight, which will be defined later. The objective of (11) is twofold:

- Unlike [19], where the TV penalty is applied only to consecutive elements, our approach extends it to a broader set of adjacent neighbors. Thus, enhancing the model's adaptability to the signal structure while effectively capturing local dependencies among its elements.
- By incorporating an adaptive regularization weight, the proposed solution can better explore the hyper-parameter space, allowing it to distinguish between nonzero blocks and isolated nonzero elements more effectively.

B. Hyper-Parameters Inference

Note that the optimization problem in (10) presents challenges due to its non-convex nature, which stems from both the log-determinant term and the prior distribution $p(\boldsymbol{\alpha})$. To overcome this complexity, this paper utilizes the expectation maximization (EM) approach [20] that enables efficient solution of the equation. The EM-SBL iterates between two steps, namely, the E-step and the M-step.

a) E-step: Given the estimated $\boldsymbol{\alpha}^{(l-1)}$, the **E-step** is evaluated at the lth EM iteration by averaging the joint posterior distribution $p(\mathbf{y}, \mathbf{z}, \boldsymbol{\alpha})$ with respect to the hidden variable $\mathbf{z}$ as

$$
\begin{aligned}
Q(\boldsymbol{\alpha}^{(l)}|\boldsymbol{\alpha}^{(l-1)}) &\overset{(a)}{=} \mathbb{E}_{p(\mathbf{y}|\mathbf{z},\boldsymbol{\alpha}^{(l-1)})}\Big[\log p(\mathbf{y}|\mathbf{z})p(\mathbf{z}|\boldsymbol{\alpha})p(\boldsymbol{\alpha})\Big] \\
&\overset{(b)}{=} \mathbb{E}_{p(\mathbf{z}|\mathbf{y},\boldsymbol{\alpha}^{(l-1)})}\Big[\log p(\mathbf{z}|\boldsymbol{\alpha}) + \log p(\boldsymbol{\alpha})\Big] \\
&\propto -\sum_{i=1}^{N}\left[\log(\alpha_i) - \frac{s_i^{(l-1)}}{\alpha_i}\right] + \log p(\boldsymbol{\alpha}),
\end{aligned} \tag{12}
$$

where $s_i^{(l-1)} = \boldsymbol{\Sigma}_{i,i}^{(l-1)} + \|\mu_i^{(l-1)}\|^2$, (a) follows from the factorization of joint distribution $\boldsymbol{\alpha} \to \mathbf{z} \to \mathbf{y}$ and (b) follows from the prior model in (7) and the fact that $p(\mathbf{y}|\mathbf{z})$ does not depend on $\boldsymbol{\alpha}$.

b) M-step: The hyper-parameter $\boldsymbol{\alpha}$ is updated as follows

$$
\begin{aligned}
\hat{\boldsymbol{\alpha}} &= \underset{\boldsymbol{\alpha}}{\operatorname{argmin}} -Q(\boldsymbol{\alpha}^{(l)}|\boldsymbol{\alpha}^{(l-1)}) \\
&= \underset{\boldsymbol{\alpha}}{\operatorname{argmin}} \sum_{i=1}^{N}\log(\alpha_i) + \frac{s_i^{(l-1)}}{\alpha_i} + \sum_{i=2}^{N}\sum_{j=1}^{i-1}\beta_{i,j}|\log(\alpha_i) - \log(\alpha_j)|,
\end{aligned} \tag{13}
$$

As mentioned earlier, the role of $\beta_{i,j}$ is to adjust the penalty applied to the pair $\{\alpha_i, \alpha_j\}$ as follows

$$
\beta_{i,j}^{(l)} = \begin{cases} \exp\left(-\|\log(\alpha_i^{(l-1)}) - \log(\alpha_j^{(l-1)})\|^2\right), & \text{if } j \in \Omega_i \\ 0, & \text{otherwise.} \end{cases} \tag{14}
$$

The key rationale behind this choice of $\beta_{i,j}$ can be summarized as follows:

- When z_i and z_j share the same sparsity profile, $\beta_{i,j}$ is set high to reinforce the smoothing effect of the TV penalty, promoting a structured block-sparse pattern.
- When z_i and z_j exhibit different sparsity profiles, setting $\beta_{i,j} \approx 0$ effectively decouples them in the optimization process, allowing independent updates and preserving their distinct characteristics.

C. ADMM solution for the M-step

Note that the problem (13) is non-convex, it is possible to utilize decomposition techniques and ADMM to obtain closed-form solution to (13) as we describe next[1].

First, we transform (13) into bi-convex optimization problem by introducing the auxiliary variable $\mathbf{C} \in \mathbb{R}^{N\times N}$ as

$$
\begin{aligned}
&\underset{\boldsymbol{\alpha},\mathbf{C}}{\operatorname{argmin}} \sum_{i=1}^{N}\log(\alpha_i) + \frac{s_i}{\alpha_i} + \sum_{i=2}^{N}\sum_{j=1}^{i-1}|C_{i,j}| \\
&\text{s.t. } C_{i,j} = \beta_{i,j}\big(\log(\alpha_i) - \log(\alpha_j)\big), \forall i,j.
\end{aligned} \tag{15}
$$

Subsequently, we write the augmented Lagrangian function as

$$
\begin{aligned}
\mathcal{L}(\boldsymbol{\alpha},\mathbf{c}) &= \sum_{i=1}^{N}\log(\alpha_i) + \frac{s_i}{\alpha_i} \\
&+ \sum_{i=2}^{N}\sum_{j=1}^{i-1}\left[|C_{i,j}| + \frac{\rho}{2}\|C_{i,j} - \bar{\alpha}_{i,j} + \frac{\lambda_{i,j}}{\rho}\|^2\right],
\end{aligned} \tag{16}
$$

where $\bar{\alpha}_{i,j} = \beta_{i,j}\Big(\log(\alpha_i) - \log(\alpha_j)\Big)$, $\boldsymbol{\lambda} \in \mathbb{R}^{N\times N}$ denotes the dual variable matrix, and ρ is a real small positive variable.

[1]from here onward, we will omit the EM iteration index (l) for sake of presentation clarity.

1) $\boldsymbol{\alpha}$-update: First, we update each element of the hyper-parameter vector sequentially as

$$
\begin{aligned}
\alpha_i^{(k+1)} &= \underset{\alpha_i}{\operatorname{argmin}} \log(\alpha_i) + \frac{\rho}{2}\sum_{\substack{j\in\Omega_i \\ j<i}}\|\tilde{a}_j^{(k)} - \beta_{i,j}\log(\alpha_i)\|^2 \\
&+ \frac{\rho}{2}\sum_{\substack{j\in\Omega_i \\ j>i}}|\bar{a}_j^{(k)} + \beta_{i,j}\log(\alpha_i)\|^2 + \frac{s_i}{\alpha_i},
\end{aligned} \tag{17}
$$

where $\tilde{a}_j^{(k)} = C_{i,j}^{(k)} + \beta_{i,j}\log(\alpha_j^{(k)}) + \frac{\lambda_{i,j}^{(k)}}{\rho}$ and $\bar{a}_j^{(k)} = C_{j,i}^{(k)} - \beta_{i,j}\log(\alpha_j^{(k)}) + \frac{\lambda_{j,i}^{(k)}}{\rho}$. An approximate solution to (17) is given as

$$
\alpha_i^{(k+1)} = s_i\Big(1 + \rho\sum_{j\in\Omega_i}\beta_{i,j} - \rho\Big(\sum_{j\in\Omega_i, j<i}\tilde{a}_j^{(k)} - \sum_{j\in\Omega_i, j>i}\bar{a}_j^{(k)}\Big)\Big)^{-1}. \tag{18}
$$

2) $\mathbf{C}$-update: Note that for solving (16), each element $C_{i,j}$ can be updated separately as

$$
C_{i,j}^{(k+1)} = \underset{C_{i,j}}{\operatorname{argmin}}\,|C_{i,j}| + \frac{\rho}{2}\|C_{i,j} - \bar{\alpha}_{i,j}^{(k+1)} + \frac{\lambda_{i,j}^{(k)}}{\rho}\|, \tag{19}
$$

where $\bar{\alpha}_{i,j}^{(k+1)} = \beta_{i,j}\big(\log(\alpha_i^{(k+1)}) - \log(\alpha_j^{(k+1)})\big)$, leading to the soft-thresholding solution [21] as

$$
C_{i,j}^{(k+1)} = \max\left(\bar{\alpha}_{i,j}^{(k+1)} - \frac{\lambda_{i,j}^{(k)}}{\rho}, 0\right) \tag{20}
$$

3) λ-update: Finally, the dual variable is update as

$$
\lambda_{i,j}^{(k+1)} = \lambda_{i,j}^{(k)} + \rho\Big(C_{i,j}^{(k+1)} - \bar{\alpha}_{i,j}^{(k+1)}\Big), \forall i,j \tag{21}
$$

IV. Simulation Results

This section presents simulation results to assess the proposed solution's performance. We set the number of BS antennas $N = 512$, the carrier frequency $f_c = 30$ GHz, the number of total paths $P = 8$. The angle of arrival and the distance between the BS and the UEs are randomly drawn from uniform distribution as $\theta \sim \mathcal{U}(-\frac{\pi}{3}, \frac{\pi}{3})$ and $r[m] \sim \mathcal{U}(10, 150)$, respectively. The pilot matrix $\mathbf{W}$ is drawn from an i.i.d. complex Bernoulli distribution with normalized columns. Performance is assessed using the normalized mean square error (NMSE), defined as $\frac{\mathbb{E}\left[\|\mathbf{h}-\hat{\mathbf{h}}\|^2\right]}{\mathbb{E}[\|\mathbf{h}\|^2]}$.

The proposed method is compared against five benchmark approaches: far-field OMP, near-field OMP [3], hybrid-field OMP with unknown path partition [12], hybrid-field OMP with known partition [11], and non-uniform burst SBL [4] [2].

Fig. 3 (a) presents the NMSE of the algorithms as a function of SNR, with $T = 128$, $P_f = 4$, and $P_n = 4$. Notably, the proposed algorithm achieves the best channel estimation accuracy across the entire SNR range, outperforming the next-best algorithm by approximately 2–3 dB. The results also indicate that algorithms designed for hybrid-channel models outperform those based on a uni-field assumption.

[2]The simulation code and implementation details for the proposed solution are available on the following GitHub repository

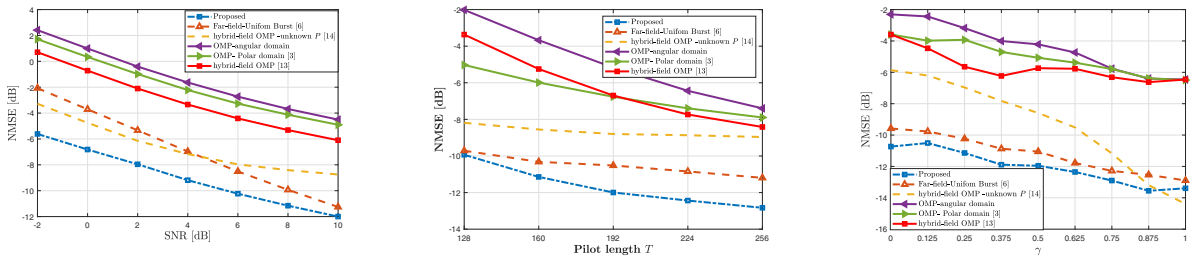

(a) (b) (c)

Fig. 3: Channel estimation performance in terms of NMSE versus (a) SNR, (b) pilot length (T), and (c) proportion of near and far-field components (γ).

Fig. 3 (b) illustrates NMSE versus received signal length (T) at SNR $= 8$ dB. Again, the proposed algorithm consistently demonstrates superior performance, significantly outperforming all benchmarks. Moreover, with a 25% shorter pilot length ($T = 192$), it achieves the same performance as the non-uniform burst algorithm at $T = 256$, yielding a 25% improvement in pilot efficiency.

Finally, we evaluate algorithm performance under varying proportions of near-field and far-field components, with SNR $= 8$ dB and $T = 128$. Let us define $\gamma \in [0, 1]$ that denotes the proportion of the near-field and far field components such that $P_{\mathrm{f}} = \lfloor \gamma P \rfloor$ and $P_{\mathrm{f}} = P - P_{\mathrm{f}}$. The results show that as γ increases—indicating a channel dominated by far-field components—performance improves across all algorithms. This is attributed to the increased sparsity of the far-field representation compared to the near-field. Once again, the proposed algorithm exhibits superior accuracy and robustness across different channel conditions.

V. Acknowledgment

This work has been supported by the Research Council of Finland (6GWiCE, grant 319485) and (6G Flagship program, grant 369116) and NSF (grant 2225617).

VI. Conclusion

In this paper, we deployed an adaptive SBL-based hybrid-field channel estimator with a flexible prior function that effectively accommodates various hybrid-field conditions. Furthermore, unlike existing works, the proposed solution does not require any knowledge of path numbers or far-field/near-field component proportions. Extensive simulations demonstrated significant performance gains compared to state-of-the-art benchmarks, highlighting the practical value of our approach for next-generation communication systems.

References

[1] Z. Wang, J. Zhang, H. Du, D. Niyato, S. Cui, B. Ai, M. Debbah, K. B. Letaief, and H. V. Poor, "A tutorial on extremely large-scale MIMO for 6G: Fundamentals, signal processing, and applications," *IEEE Communications Surveys & Tutorials*, vol. 26, no. 3, pp. 1560–1605, 2024.

[2] Z. Wang, J. Zhang, H. Du, E. Wei, B. Ai, D. Niyato, and M. Debbah, "Extremely large-scale MIMO: Fundamentals, challenges, solutions, and future directions," *IEEE Wireless Commun. Mag.*, 2023.

[3] M. Cui and L. Dai, "Channel estimation for extremely large-scale MIMO: Far-field or near-field?" *IEEE Trans. Commun.*, vol. 70, no. 4, pp. 2663–2677, 2022.

[4] J. Dai, A. Liu, and H. C. So, "Non-uniform burst-sparsity learning for massive MIMO channel estimation," *IEEE Trans. Signal Processing*, vol. 67, no. 4, pp. 1075–1087, 2018.

[5] C. Huang, L. Liu, C. Yuen, and S. Sun, "Iterative channel estimation using LSE and sparse message passing for mmWave MIMO systems," *IEEE Trans. Signal Processing*, vol. 67, no. 1, pp. 245–259, 2018.

[6] Y. Lu and L. Dai, "Near-field channel estimation in mixed LoS/NLoS environments for extremely large-scale MIMO systems," *IEEE Trans. Wireless Commun.*, vol. 71, no. 6, pp. 3694–3707, 2023.

[7] X. Zhang, Z. Wang, H. Zhang, and L. Yang, "Near-field channel estimation for extremely large-scale array communications: A model-based deep learning approach," *IEEE Commun. Lett.*, vol. 27, no. 4, pp. 1155–1159, 2023.

[8] H. Lei, J. Zhang, H. Xiao, X. Zhang, B. Ai, and D. W. K. Ng, "Channel estimation for XL-MIMO systems with polar-domain multi-scale residual dense network," *IEEE Trans. Veh. Commun.*, vol. 73, no. 1, pp. 1479–1484, 2023.

[9] Z. Hu, C. Chen, Y. Jin, L. Zhou, and Q. Wei, "Hybrid-field channel estimation for extremely large-scale massive MIMO system," *IEEE Commun. Lett.*, vol. 27, no. 1, pp. 303–307, 2022.

[10] H. Lei, J. Zhang, Z. Wang, B. Ai, and D. W. K. Ng, "Hybrid-field channel estimation for XL-MIMO systems with stochastic gradient pursuit algorithm," *IEEE Trans. Signal Processing*, 2024.

[11] X. Wei and L. Dai, "Channel estimation for extremely large-scale massive MIMO: Far-field, near-field, or hybrid-field?" *IEEE Commun. Lett.*, vol. 26, no. 1, pp. 177–181, 2021.

[12] W. Yang, M. Li, and Q. Liu, "A practical channel estimation strategy for XL-MIMO communication systems," *IEEE Commun. Lett.*, vol. 27, no. 6, pp. 1580–1583, 2023.

[13] J. Xiao, J. Wang, Z. Chen, and G. Huang, "U-MLP-based hybrid-field channel estimation for XL-RIS assisted millimeter-wave MIMO systems," *IEEE Wireless Communications Letters*, vol. 12, no. 6, pp. 1042–1046, 2023.

[14] X. Yan and J. Yuan, "Dynamic hybrid-field channel estimation for extremely large-scale massive MIMO," in *Proc. IEEE Wireless Commun. and Networking Conf.* IEEE, 2024, pp. 1–6.

[15] J. Ziniel and P. Schniter, "Efficient high-dimensional inference in the multiple measurement vector problem," *IEEE Trans. Signal Processing*, vol. 61, no. 2, pp. 340–354, 2012.

[16] E. Björnson, J. Hoydis, and L. Sanguinetti, "Massive MIMO networks: Spectral, energy, and hardware efficiency," *Foundations and Trends® in Signal Processing*, vol. 11, no. 3-4, pp. 154–655, 2017.

[17] H. Djelouat, R. Leinonen, M. J. Sillanpää, B. D. Rao, and M. Juntti, "Adaptive and self-tuning SBL with total variation priors for block-sparse signal recovery," 2025. [Online]. Available: https://arxiv.org/abs/2503.09290

[18] J. Fang, Y. Shen, H. Li, and P. Wang, "Pattern-coupled sparse Bayesian learning for recovery of block-sparse signals," *IEEE Trans. Signal Processing*, vol. 63, no. 2, pp. 360–372, 2014.

[19] A. Sant, M. Leinonen, and B. D. Rao, "Block-sparse signal recovery via general total variation regularized sparse Bayesian learning," *IEEE Trans. Signal Processing*, vol. 70, pp. 1056–1071, 2022.

[20] D. P. Wipf and B. D. Rao, "Sparse Bayesian learning for basis selection," *IEEE Trans. Signal Processing*, vol. 52, no. 8, pp. 2153–2164, 2004.

[21] T. Goldstein, C. Studer, and R. Baraniuk, "A field guide to forward-backward splitting with a FASTA implementation," *arXiv preprint arXiv:1411.3406*, 2014.